Available online at www.sciencedirect.com
SCIENCE DIRECT®
Journal of Sound and Vibration 284 (2005) 1–22
JOURNAL OF SOUND AND VIBRATION
www.elsevier.com/locate/jsvi

Modal response of a beam with a sensor–actuator pair for the implementation of velocity feedback control

Paolo Gardonio*, Stephen J. Elliott

Institute of Sound and Vibration Research, University of Southampton, Highfield, Southampton SO17 1BJ, UK

Received 2 October 2003; accepted 4 June 2004
Available online 25 November 2004

Abstract

A theoretical analysis is presented of the flexural vibration of a beam with a control system which implements direct velocity feedback using either an ideal collocated force actuator or a closely located piezoelectric patch actuator. The aim of this study is to describe the vibration of the beam as the control gain is raised. Both control systems generate active damping which reduces the vibration level at resonance frequencies. However, it is shown that when the gain passes an optimal value then the vibration of the beam is rearranged into a new set of lightly damped resonance frequencies, since the control systems impose new boundary conditions at the control position on the beam, in which the velocity is driven to zero in both cases but different spatial derivatives of the velocity are driven to zero in the case of the force actuator and the piezoelectric patch actuator.

The new ''natural frequencies'' and ''natural modes'' of the beam constrained by the two feedback control systems with large control gains are derived analytically. The new resonance frequencies and mode shapes seen in the simulations are consistent with the natural frequencies and natural modes of the constrained beams derived analytically.

*Corresponding author. Tel.: +44-23-8059-4933; fax: +44-23-8059-3190.
E-mail address: pg@isvr.soton.ac.uk (P. Gardonio).

0022-460X/$ - see front matter © 2004 Elsevier Ltd. All rights reserved.
doi:10.1016/j.jsv.2004.06.018

1. Introduction

This paper presents a theoretical analysis of the new flexural natural frequencies and natural modes of a beam generated by a control system which implements direct velocity feedback (DVFB), i.e. active damping, using either an ideal collocated or a practical closely located sensor actuator pairs with relatively high feedback control gains.

Active damping of flexible distributed systems was first introduced a long time ago [1–3]. Since then several studies have been presented with different active control approaches based on: (a) direct velocity feedback, (b) acceleration feedback and (c) positive position feedback. A comprehensive review of these feedback control schemes for the implementation of active damping in flexible structures is given in by Preumont [4]. DVFB could be considered to be the simplest way to implement active damping since the velocity signal measured by a sensor is electronically multiplied by a fixed gain and feed directly feedback to an actuator. Balas [5], and Benhabib et al. [6] showed that, if (a) the number of sensors is equal to the number of actuators, (b) only velocity (rate) sensors are used, (c) the actuators and sensors are collocated and (d) the actuators do not excite rigid-body modes, then the control scheme is guaranteed to be stable since the closed-loop system with DVFB is energy dissipative, i.e. it is passive.

This study follows from a previous research work on a smart panel for broad-band low-frequency reduction of the panel flexural vibration and sound radiation/transmission using an array of decentralized active damping control systems [7–11]. The smart panel is clamped along the perimeter and is equipped with an array of closely located accelerometer sensor–piezoelectric patch actuator pairs that implement decentralized DVFB control loops with the same control gains. Although these sensor–actuator pairs are not collocated and dual [12,13], it has been shown that these decentralized control systems are conditionally stable [8,10] and could be used to generate active damping so that as the equivalent control gains are raised as the vibration of the panel is gradually reduced at resonance frequencies. As a result the averaged low-frequency response and sound radiation of the panel due to a broad-band random excitation are also reduced [7,9,11]. The dissipative effect monotonically grows until an optimal control gain is reached [7,9]. If the control gains are further increased then the damping effects gradually fade away and the frequency averaged vibration and sound radiation monotonically rises to the same or even higher values than those of the panel with no control. The simulation analysis presented in Ref. [7,9] shows that for higher control gains than the optimal one, the vibration and sound radiation of the panel is characterized by a new set of lightly damped resonances which cause the growth of the frequency averaged vibration and frequency averaged sound radiation of the panel. This phenomenon is due to the fact that for relatively higher control gains the panel is constrained by the control system so that little active damping can be generated. The vibration of the panel is therefore rearranged to that of a lightly damped panel that is constrained in a way that depends on the nature of the control system. These additional constraints change the flexural mode shapes and the natural frequencies of the panel.

This type of phenomenon is well known in the control literature but is usually discussed with reference to stability issues. Fundamental text books on feedback control of dynamic systems, as for example those by Meirovitch [14] and Franklin et al. [15], present the root-locus method for single-input single-output feedback control and highlight the fact that as the control gain is raised as the closed-loop poles, and thus the resonance frequencies of the controlled

system, migrates from the poles to the zeros of the open-loop systems, that is from the resonance to the antiresonance frequencies of the uncontrolled system. The poles depend on the material properties and the prescribed boundary conditions of the mechanical system. Alternatively, the zeros depend on the positions and types of the sensor and actuator [4,16–20]. Martin [16] showed that the transfer function of a collocated sensor–actuator pair has alternating poles and zeros along the imaginary axis in the root-locus plot so that, in absence of sensor/actuator dynamics, a rate feedback control system is guaranteed to be stable. Preumont [4], highlights that stable rate feedback is guaranteed for any location of the sensor–actuator pair(s) even though the higher are the controllability and observability (in collocated control they go together) for a given mode of the system, the bigger is the corresponding loop in the root-locus plot and thus larger damping effects can be achieved. Indeed the maximum active damping effect on each mode of the system is given by an intermediate optimal gain that is directly proportional to the difference between the corresponding resonance (open-loop pole) and antiresonance (open-loop zero) frequencies and inversely proportional to twice the resonance frequencies of the open-loop system.

The theory and analysis of DVFB control was developed mainly for position control problems related to flexible closed chain or open chain (robots) mechanisms. Emphasis was therefore given to the objective of getting good control performance at a specific position of the system, as for example position control of a robot's arm, and most of the analysis was addressed to the stability problem. That is probably why the modal reconstruction phenomenon described above has not been studied in great detail and, at best knowledge of the authors, relatively few publications are devoted to it as for example those listed in Ref. [16–20]. The problem of controlling the sound radiation of one- or two- dimensional structures vibrating in flexure does instead require a good understanding of the physics of DVFB: in particular, it calls for a fine comprehension of the modal response of the structure which would give an insight to the self and mutual radiation of sound by the modes of the constrained structure [21,22].

The aim of this paper is therefore to derive and analyse the new ''natural frequencies'' and ''natural modes'' generated by very high control gains of a DVFB control system in such a way as to provide a physical interpretation of the reduced sound radiation control effects found for the smart panels with decentralized DVFB control systems described in Ref. [7–11]. In order to present a compact analytical formulation a simpler system than the smart panel is considered, which consists of a simply supported beam excited in flexure with only one control system that implements direct velocity feedback. The beam is equipped with a DVFB control system using either a collocated force actuator and velocity sensor or a closely positioned piezoelectric patch actuator and a velocity sensor. The first is an ideal control system that is unconditionally stable, while the second is only conditionally stable, but could be used in practice to generate active damping with integrated transducers and thus reduce the vibration level at resonance frequencies [9,11,23]. For relatively large control gains the two control systems rearrange the vibration of the beam into a new set of lightly damped resonance frequencies, since the control systems impose new boundary conditions at the control position on the beam in which the velocity is driven to zero in both cases but different spatial derivatives of the velocity are driven to zero in the case of the force actuator and piezoelectric patch actuator. As a result, for relatively high control gains the vibration of the actively controlled beam can be described in terms of a new set of ''natural frequencies'' and ''natural modes''.

The study is subdivided in two parts. The first part describes a mobility model used to derive the flexural response of the beam with the two types of control systems when it is excited by a plane acoustic wave. Simulations results are presented which show (a) the total kinetic energy of the beam in a frequency range between 0 and 1 kHz for a set of control gains and (b) the 0–1 kHz frequency averaged total kinetic energy as a function of the control gain. Also, the vibration profile along the beam length is shown for the first four unconstrained and actively constrained resonance frequencies of the beam. The second part of the paper presents an analytical formulation for the new natural frequencies and natural modes of the beam with the additional constraints generated by the two types of control systems. In the appendix an alternative formulation is also given for the derivation of the new natural frequencies and natural modes of the actively constrained beam based on the mode-summation procedure for continuous flexible systems. This is an approximate approach which however enables the calculus of the new natural frequencies and natural modes for any value of the feedback control gain.

2. Mobility model

The system studied in this paper consists of a simply supported beam with either a collocated ideal velocity sensor and force actuator direct feedback control system or a practical closely located velocity sensor and piezoelectric patch actuator direct feedback control system as shown in Figs. 1a and b, respectively. The steady-state transverse vibration of the beam in a frequency range 0–1 kHz has been calculated assuming the primary disturbance to be a plane acoustic wave at an angle $\theta = 45^\circ$ with harmonic time dependence of the form $\exp(j\omega t)$. The velocity, force and moments pair functions used in the model have been taken to be the real part of counterclockwise rotating complex vectors, so that $\dot{w}(t) = \mathrm{Re}\{\dot{w}(\omega)e^{j\omega t}\}$, $f(t) = \mathrm{Re}\{f(\omega)e^{j\omega t}\}$ and $m(t) = \mathrm{Re}\{m(\omega)e^{j\omega t}\}$ where $\dot{w}(\omega)$, $f(\omega)$ and $m(\omega)$ are the complex velocity and force or moments-pair phasors at $t = 0$, ω is the circular frequency and $j = \sqrt{-1}$.

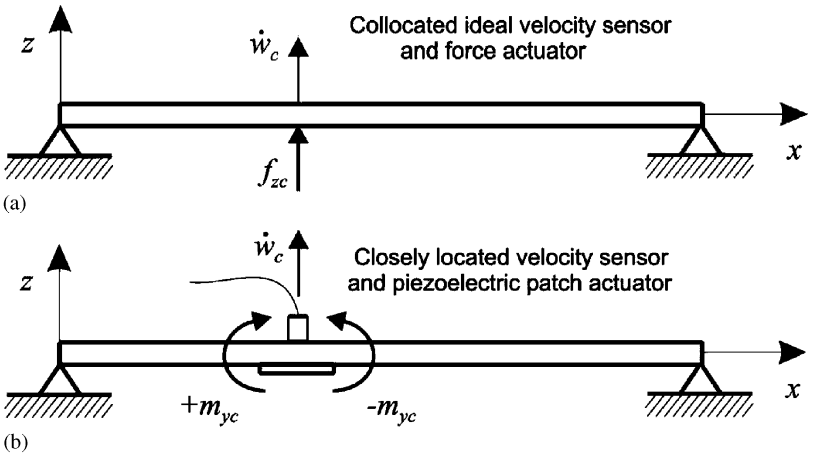

Fig. 1. Simply supported beam with (a) an ideal collocated velocity sensor and force actuator and (b) a practical closely located velocity sensor and piezoelectric patch actuator.

The phasors of the transverse velocities along the beam length, $\dot{w}_b(x,\omega)$, and at the error sensor position, $\dot{w}_c(\omega)$, could be expressed in terms of the primary and secondary excitations as follows:

$$\dot{w}_b(x,\omega) = Y_{bp}(x,\omega)p_p(\omega) + Y_{bc}(x,\omega)u_c(\omega), \tag{1}$$

$$\dot{w}_c(\omega) = Y_{cp}(\omega)p_p(\omega) + Y_{cc}(\omega)u_c(\omega), \tag{2}$$

where $p_p(\omega)$ is the phasor of the acoustic pressure of the incident primary wave and $u_c(\omega)$ is the phasor of the control excitation which could be either the control force or the control moments pair which are denoted $f_{zc}(\omega)$ and $m_{yc}(\omega)$, respectively, in Fig. 1. The stiffening and mass effects of the piezoelectric patch actuator will not be taken into account in the model, therefore the four mobility terms in Eqs. (1) and (2) are given by the following formulae:

$$Y_{bp}(x,\omega) = \boldsymbol{\phi}(x)\mathbf{a}_p(\omega), \quad Y_{bc}(x,\omega) = \boldsymbol{\phi}(x)\mathbf{a}_c(\omega), \tag{3,4}$$

$$Y_{cp}(\omega) = \boldsymbol{\phi}(x_c)\mathbf{a}_p(\omega), \quad Y_{cc}(\omega) = \boldsymbol{\phi}(x_c)\mathbf{a}_c(\omega), \tag{5,6}$$

where $\phi(x)$ are row vectors with the first R flexural natural modes of the beam

$$\boldsymbol{\phi}(x) = \begin{bmatrix}\phi_1(x) & \phi_2(x) & \cdots & \phi_R(x)\end{bmatrix} \tag{7}$$

and $\mathbf{a}_p(\omega)$, $\mathbf{a}_c(\omega)$ are column vectors of the excitation terms of the first R flexural natural modes of the unconstrained beam due to either the primary or control excitations:

$$\mathbf{a}_p(\omega) = \begin{bmatrix} a_{p,1}(\omega) \\ a_{p,2}(\omega) \\ \vdots \\ a_{p,R}(\omega)\end{bmatrix}, \quad \mathbf{a}_c(\omega) = \begin{bmatrix} a_{c,1}(\omega) \\ a_{c,2}(\omega) \\ \vdots \\ a_{c,R}(\omega)\end{bmatrix}. \tag{8,9}$$

The terms in the primary excitation vector, $\mathbf{a}_p(\omega)$, are given by

$$a_{p,r}(\omega) = \frac{4l_y \int_0^{l_x} \phi_r(x)\mathrm{e}^{-\mathrm{j}k_x x}\mathrm{d}x}{M\left[\omega_r^2 - \omega^2 + \mathrm{j}2\zeta_r\omega_r\omega\right]}, \tag{10}$$

while the terms for either the force or moments pair control excitations in the control excitation vector, $\mathbf{a}_c(\omega)$, are given, respectively, by

$$a_{c,r}(\omega) = \frac{2\phi_r(x_c)}{M\left[\omega_r^2 - \omega^2 + \mathrm{j}2\zeta_r\omega_r\omega\right]}, \quad a_{c,r}(\omega) = \frac{2\left\{\phi_r'(x_c - e) - \phi_r'(x_c + e)\right\}}{M\left[\omega_r^2 - \omega^2 + \mathrm{j}2\zeta_r\omega_r\omega\right]}, \tag{11a,b}$$

where l_y is the width of the beam, $k_x = k\sin\theta$ is the trace of the acoustic wavenumber k, ω_r is the rth flexural natural frequency, $\phi_r(x)$ is the rth flexural natural mode, $\phi_r'(x) = \mathrm{d}\phi_r(x)/\mathrm{d}x$ is the first derivative in x of the rth flexural natural mode, $2e$ is the length of the piezoelectric control actuator, ζ_r is the damping factor of the rth flexural natural mode and $M = \rho A l_x$ is the mass of the beam with ρ the density of the material, A the cross-sectional area and l_x the length of the beam. The flexural natural frequencies and natural modes of a simply supported beam are given by the following formulae [24]:

$$\omega_r = \frac{r^2\pi^2}{l^2}\sqrt{\frac{EI_y}{A\rho}}, \quad \phi_r(x) = \sin\frac{r\pi x}{l}, \tag{12,13}$$

where E is Young's modulus elasticity and I_y is the cross-sectional second moment of area with reference to the y-axis. When there is no control action, i.e. $u_c(\omega) = 0$, then the transverse velocity along the beam length can be calculated directly from Eq. (1) to be

$$\dot{w}_b(x,\omega) = Y_{bp}(x,\omega)p_p(\omega). \tag{14}$$

When, as shown in the block diagram in Fig. 2, the sensor–actuator pair implements velocity feedback control with a fixed control gain h, such that

$$u_c(\omega) = -h\dot{w}_c(\omega), \tag{15}$$

then, provided the control loop is stable, the velocity at the error sensor position is given by

$$\dot{w}_c(\omega) = \frac{Y_{cp}(\omega)}{1 + hY_{cc}(\omega)}p_p(\omega) \tag{16}$$

and the transverse velocities along the beam length are given by

$$\dot{w}_b(x,\omega) = \left\{ Y_{bp}(x,\omega) - Y_{bc}(x,\omega)\frac{hY_{cp}(\omega)}{1 + hY_{cc}(\omega)} \right\} p_p(\omega). \tag{17}$$

It should be underlined that this result is valid provided the control system is stable. If the sensor–actuator transducers are collocated and dual, i.e. the detection and excitation of a point sensor–actuator pair occurs for the same degree of freedom [12], then the sensor–actuator response function is constrained to be positive real [5,6]. Therefore the denominator of Eq. (16) is always positive and greater than one so that the ratio $\dot{w}_c(\omega)/p_p(\omega)$ is monotonically reduced as the control gain h is raised and thus the feedback control loop in Fig. 2 is guaranteed to be unconditionally stable.

The overall flexural vibration level of the beam has been represented in term of the total kinetic energy

$$T(\omega) = \frac{1}{2}\int_0^{l_x} \rho A|\dot{w}(x,\omega)|^2 \,\mathrm{d}x, \tag{18}$$

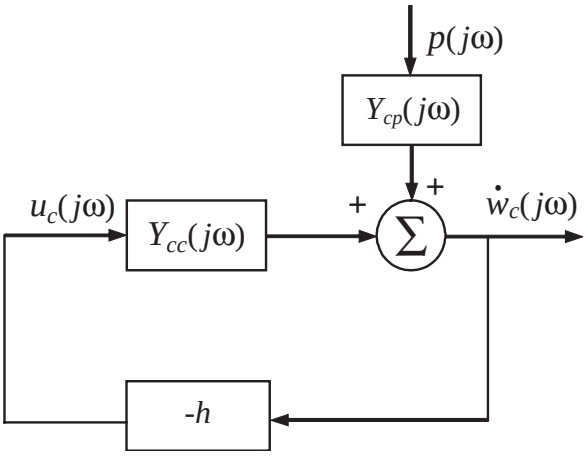

Fig. 2. Block diagram of feedback control system implemented in the beam.

which, using Eqs. (14) and (17), becomes, respectively, for the cases with and without feedback control:

$$T(\omega) = \tfrac{1}{4} M p_p^*(\omega) \mathbf{a}_p^{\mathrm{H}}(\omega) \mathbf{a}_p(\omega) p_p(\omega) \tag{19}$$

and

$$T_c(\omega) = \tfrac{1}{4} M p_p^*(\omega) \left[\mathbf{a}_p^{\mathrm{H}}(\omega) + \mathbf{a}_{fc}^{\mathrm{H}}(\omega) \right] \left[\mathbf{a}_p(\omega) + \mathbf{a}_{fc}(\omega) \right] p_p(\omega), \tag{20}$$

where * denotes the conjugate and H denotes the Hermitian transpose. $\mathbf{a}_{fc}$ is the column vector with the modal excitation terms generated by the control systems which, using Eqs. (15) and (16), is found to be given by the following relation:

$$\mathbf{a}_{fc}(\omega) = \mathbf{a}_c(\omega) \frac{h Y_{cp}(\omega)}{1 + h Y_{cc}(\omega)}. \tag{21}$$

With this formulation it has been possible to derive (a) the total flexural kinetic energy between 0 and 1 kHz; (b) the 0–1 kHz frequency averaged total flexural kinetic energy for a range of control gains between 0.01 and 1000 and (c) the flexural vibration amplitude along the beam length at specific frequencies. These three types of results can be used to describe the control effects and the consequent rearrangement of the modal response of the beam when higher gains are implemented with the two control systems. The dimensions and the material properties of the beam considered in this study are summarized in Table 1. In order to better highlight the modal response of the beam a relatively low damping ratio of 0.1% has been used. With such a low damping, the forced response of the beam at a resonance frequency is dominated by the resonant natural mode.

2.1. Active damping with the collocated velocity sensor and force actuator

The total flexural kinetic energy of the beam excited by the primary acoustic plane wave is shown in Fig. 3 for a frequency range between 0 and 1 kHz. On the top part of the plot, the modulus of the velocity sensor frequency response function, $Y_{cc}(\omega)$, when driven by the force actuator is also plotted in order to highlight the resonance frequencies of the beam and the

Table 1
Geometry and physical parameters for the beam

Parameter	Value
Length	$l_x = 300\,\mathrm{mm}$
Cross section	$l_y \times l_z = 25 \times 1\,\mathrm{mm}$
Position of the control system	$x_c = 127.5\,\mathrm{mm}$
Piezoelectric patch length	$2e = 6\,\mathrm{mm}$
Mass density	$\rho = 2700\,\mathrm{kg/m^3}$
Young's modulus	$E = 7.1 \times 10^{10}\,\mathrm{N/m^2}$
Poisson's ratio	$\nu = 0.33$
Damping ratio of the rth natural mode	$\zeta_r = 0.001$

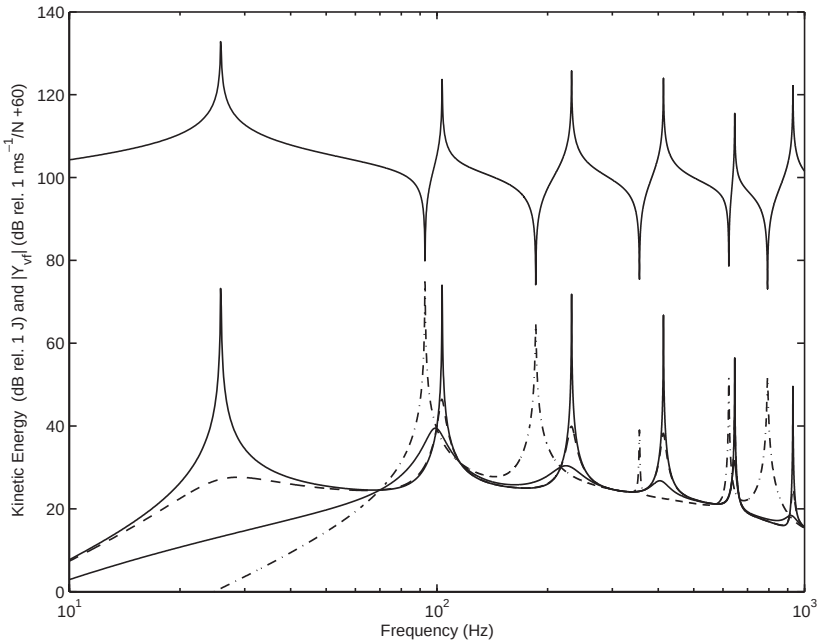

Fig. 3. Total flexural kinetic energy of the beam, when it is excited by the acoustic plane wave, with no control, thicker solid line, and with the collocated velocity sensor and force actuator feedback control system having a feedback gain of 1.05 dashed, 5.34 faint (optimal control gain), and 1000 dash–dotted lines. On the top part of the graph is plotted the modulus of the velocity sensor–force actuator frequency response function shifted by 60 dB.

Table 2
Resonance frequencies of the beam observed without control system and with either the velocity sensor and collocated force actuator or the closely located velocity sensor and piezoelectric patch actuator control systems with very high feedback control gains

Resonance number	Resonance frequency of the beam with no control system (Hz)	Resonance frequencies of the beam with the velocity sensor and force actuator (Hz)	Resonance frequencies of the beam with the velocity sensor and piezoelectric patch actuator (Hz)
1	25.8	92.8	54.6
2	103.3	185.7	117.6
3	232.5	355.6	276.9
4	413.4	622.5	498.2
5	645.7	793.3	681.3
6	930.1		

antiresonance frequencies due to this sensor–actuator pair [4,20]. This plot shows the presence of six resonance frequencies as summarized in Table 2. When the feedback control loop is closed and the control gain is gradually raised from zero, then, the collocated velocity sensor and control force actuator system progressively introduce damping at the six resonance frequencies as

highlighted by the dashed and faint lines in Fig. 3. As expected, the damping effect for a given feedback control gain is relatively large for the first resonance and tends to be smaller for the higher order resonances. The maximum reduction of the total kinetic energy, and thus the maximum damping effect, over the 0–1 kHz frequency band, is shown by the faint line in Fig. 3, corresponding to a feedback gain 5.34. If the control gain is further increased, then the vibration of the beam is rearranged into a new set of lightly damped resonances as shown by the dash–dotted line in Fig. 3 whose frequencies are listed in Table 2. Comparing this curve with the sensor–actuator frequency response function plotted above, it is clear that these new resonance frequencies correspond to the antiresonances generated by the collocated velocity sensor and force actuator.

The main features of this behaviour are summarized in Fig. 4, where the 0–1 kHz frequency averaged total kinetic energy ratio of the beam without and with feedback control is plotted against the feedback gain in a range between 10^{-5} and 10^{5} (solid line). This plot illustrates that as the control gain is gradually raised from zero as the frequency averaged total kinetic energy, and thus the overall vibration of the beam, is reduced. A maximum reduction of 16.7 dB is achieved for a control gain of 5.34. However, for higher control gains, the overall kinetic energy of the beam monotonically rises to even higher values than those of the beam with no control.

The aim of this paper is to analyse the response of the beam for very high control gains to investigate the modal response at the new resonance frequencies. Fig. 5 shows the vibration along the beam length at the first four resonance frequencies of the uncontrolled beam. The maximum

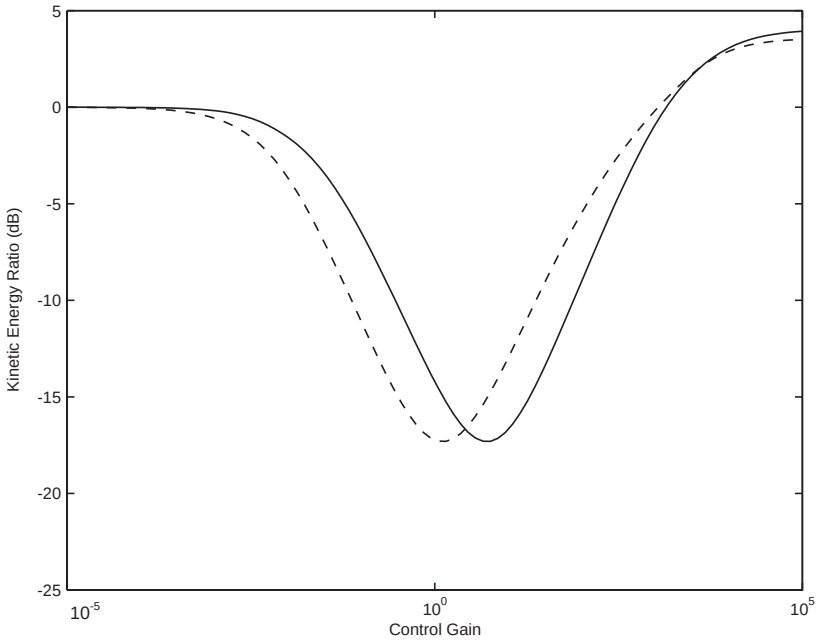

Fig. 4. Ratio of the beam total kinetic energy without and with feedback control integrated from 0–1 kHz, plotted against the gain in the feedback controller, h, for the collocated velocity sensor and force actuator control system (solid line) and the closely located velocity sensor and piezoelectric patch actuator control system (dashed line).

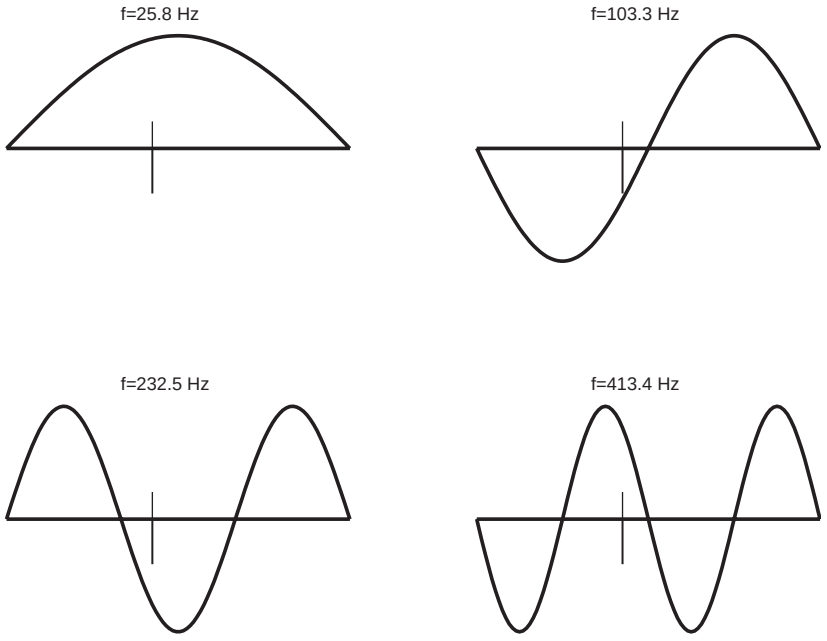

Fig. 5. Vibration of the beam excited by the plane acoustic wave at the first four resonance frequencies when there is no control.

amplitude of the four responses have all been normalized to be equal. As one would expect, the first four resonant responses of the beam are controlled by the first four flexural natural modes of the unconstrained beam given in Eq. (13). Fig. 6 shows the vibration distribution along the beam length at the first four new resonance frequencies when large control gains are implemented with the collocated velocity sensor and force actuator feedback control system. The maximum amplitude of the four responses have again been normalized to be equal. Since at resonance frequencies the response of the beam is primarily determined by the natural modes of the beam, the four plots should give a fair representation of the new mode shapes of the beam when constrained by the direct velocity feedback control system with the force actuator. For high control gains the new resonant responses of the beam are the same as those of a beam pinned at the error sensor positions.

2.2. *Active damping with the closely positioned velocity sensor and piezoelectric patch actuator*

The top part of Fig. 7 shows the modulus of the frequency response function from the piezoelectric patch actuator to the velocity sensor, $Y_{cc}(\omega)$. The piezoelectric patch actuator is modelled as a pair of moments separated by a distance of 6 mm, as described above. The resonance frequencies of the beam are the same as those above, but the antiresonance frequencies due to this sensor–actuator pair are not the same as in Fig. 3 [4,20]. When the feedback control loop is closed and the control gain is progressively raised from zero, then, the closely located velocity sensor and piezoelectric patch actuator control system gradually introduce damping at the six resonance frequencies as highlighted by the dashed and faint lines in Fig. 7. Also in this

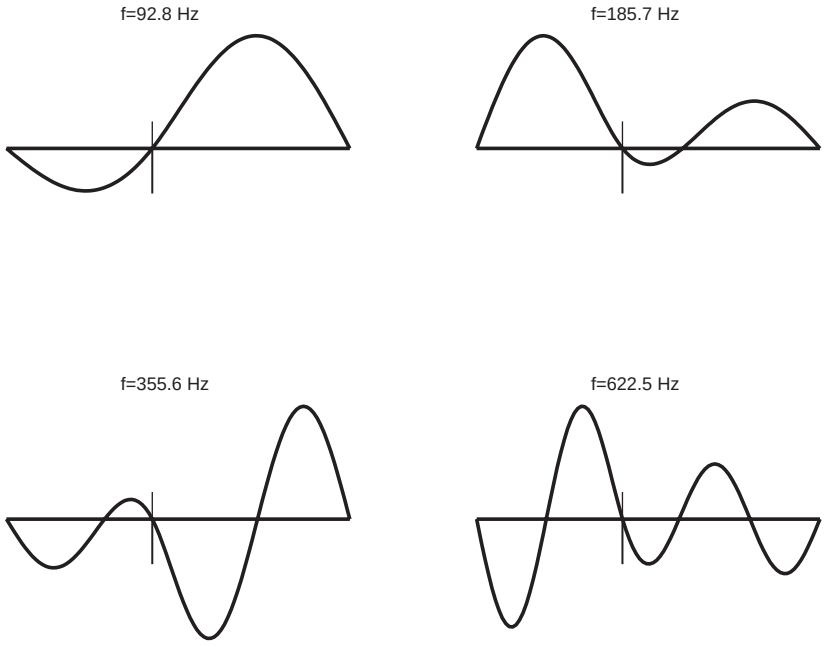

Fig. 6. Vibration of the beam excited by the plane acoustic wave at the first four new resonance frequencies when large control gains are implemented with the collocated velocity sensor and force actuator feedback control system.

case, for a given feedback gain the damping effect is relatively large for the first resonance and tends to be smaller and smaller for the higher order resonances. The maximum reduction of the total kinetic energy, and thus the maximum damping effect over the 0–1 kHz frequency band, is shown by the faint line in Fig. 7, corresponding to a feedback gain 1.32. As seen in the previous case, when the control gain is further increased then the vibration of the beam is rearranged into a new set of lightly damped resonances as shown by the dash–dotted line in Fig. 7. Comparing this curve with the sensor–actuator frequency response function plotted above, it is clear that these new resonance frequencies again correspond to the antiresonances generated by the closely located velocity sensor and piezoelectric patch actuator. As summarized in Table 2, the new resonance frequencies in this case occur for lower frequencies than those found in the previous case, with the collocated force actuator and velocity sensor.

The 0–1 kHz frequency averaged total kinetic energy ratio of the beam without and with feedback control is shown by the dashed line in Fig. 4 for a range of control gains between 10^{-5} and 10^{5}. As for the previous case, the frequency averaged total kinetic energy, and thus the overall vibration of the beam, is reduced as the control gain is increased until a maximum reduction of 16.7 dB is achieved for a control gain of 1.32, but the overall kinetic energy then rises with higher feedback gains and is greater than with no control when the new resonance dominate.

Fig. 8 shows the vibration distribution along the beam length at the first four new resonance frequencies when large control gains are implemented with the closely located velocity sensor and piezoelectric patch actuator feedback control system which, being at a resonance frequencies, should give a fair representation of the new mode shapes of the beam when constrained by

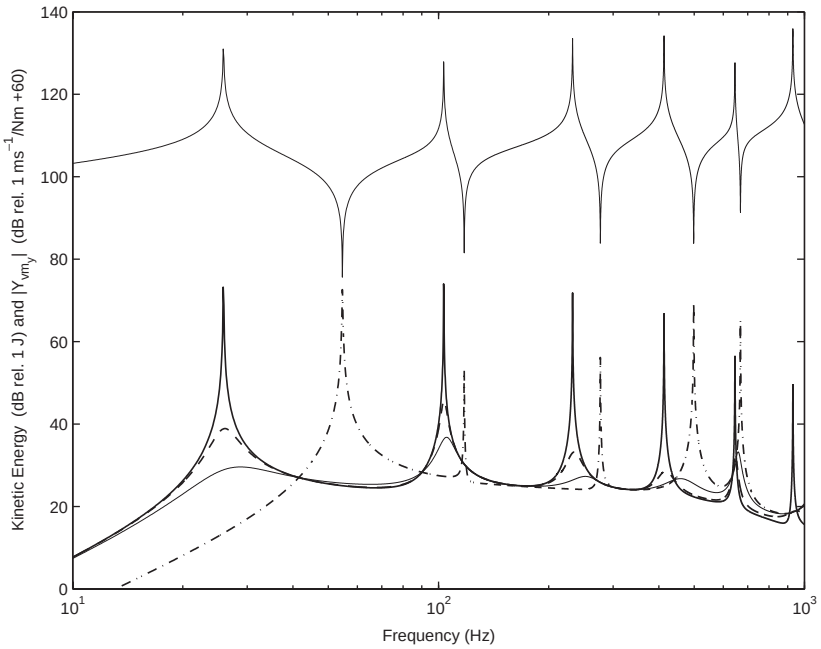

Fig. 7. Total flexural kinetic energy of the beam, when it is excited by the acoustic plane wave, with no control, thicker solid line, and with the collocated velocity sensor and piezoelectric patch actuator feedback control system having a feedback gain of 0.41, dashed, 1.32 faint (optimal control gain) and 1000 dash–dotted lines. On the top part of the graph is plotted the modulus of the velocity sensor–piezoelectric patch actuator frequency response function shifted by 60 dB.

the direct velocity feedback control system with the piezoelectric patch actuator. The maximum amplitude of the four responses have again been normalized to be equal. These plots highlight that for large control gains the new resonant responses of the beam are pinned at the error sensor positions. In this case however the moment excitation of the control actuator produce quite irregular vibration fields corresponding to no obvious boundary condition at the error sensor location.

3. Natural modes of the actively constrained beam

The natural modes of the beam when the velocity at the control position is constrained by a collocated force actuator or a closely positioned piezoelectric patch actuator are now derived analytically and compared with the vibration of the beam at the new resonance frequencies generated by the control systems with relatively high control gains which, for the relatively low damping ratio considered in this study, should give a fair representation of the natural modes. The wave equation for free flexural vibrations in a beam is given by [24]

$$EI_y \frac{\partial^4 w(x,t)}{\partial x^4} + \rho A \frac{\partial^2 w(x,t)}{\partial t^2} = 0, \tag{22}$$

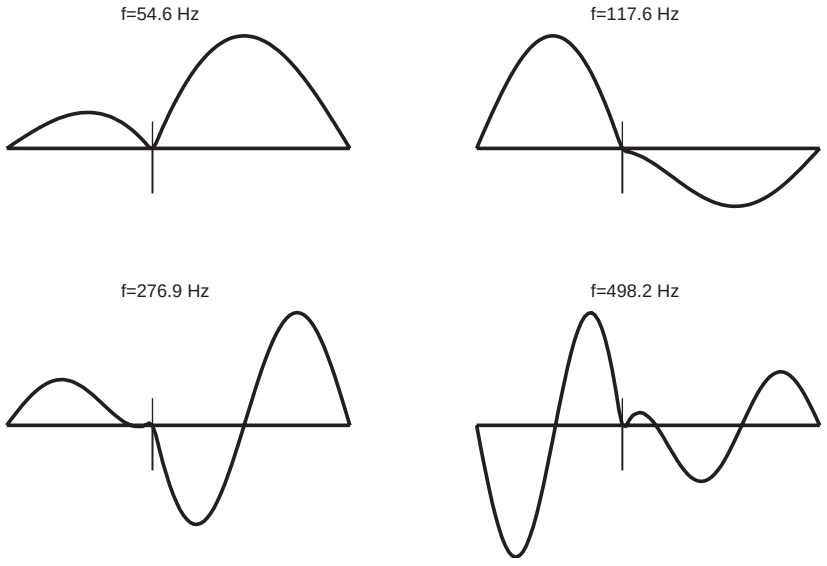

Fig. 8. Vibration of the beam excited by the plane acoustic wave at the first four new resonance frequencies when large control gains are implemented with the closely located velocity sensor and piezoelectric patch actuator feedback control system.

which, assuming harmonic vibration in the form $w(x,t) = \mathrm{Re}\{\phi(x)e^{j\omega t}\}$ and supposing the time-dependent term $\exp(j\omega t)$ to be implicit in all expressions, becomes

$$\frac{d^4\phi(x)}{dx^4} - \beta^4\phi(x) = 0, \tag{23}$$

where $\beta = \sqrt{\omega}\sqrt[4]{\rho A/(y)EI}$. The solution of this fourth order differential equation can be written in the form

$$\phi(x) = A\cosh\beta x + B\sinh\beta x + C\cos\beta x + D\sin\beta x. \tag{24}$$

3.1. Beam with the collocated velocity sensor and force actuator feedback control system

The natural modes of the controlled beam with the collocated velocity sensor and force actuator as $h \to \infty$ can be derived by dividing the beam into two bays with the two mirror systems of reference x_1 and x_2 as shown in Fig. 9. The boundary conditions for the two bays are as follows:

$$\phi_1(0) = 0, \quad \left.\frac{d^2\phi_1(x_1)}{dx_1^2}\right|_{x_1=0} = 0, \quad \phi_1(l_1) = 0, \tag{25a–c}$$

$$\phi_2(0) = 0, \quad \left.\frac{d^2\phi_2(x_2)}{dx_2^2}\right|_{x_2=0} = 0, \quad \phi_2(l_2) = 0, \tag{26a–c}$$

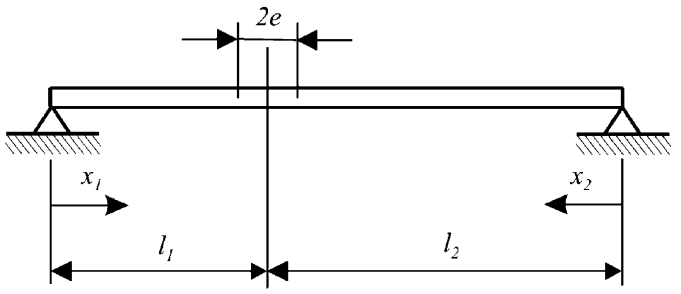

Fig. 9. Simply supported beam divided into two elements with the left to right x_1 system of reference and the right to left x_2 system of reference.

which define the simply supported ends of the beam and the fact that the velocity is driven to zero at the control point. Imposing the two boundary conditions for $x_1=0$ and $x_2=0$ it is found that

$$A_1 = C_1 = 0, \quad A_2 = C_2 = 0 \tag{27a,b}$$

and setting the other two boundary conditions for $x_1=l_1$ and $x_2=l_2$ the spatial functions $\phi_1(x_1)$ and $\phi_2(x_2)$ becomes

$$\phi_1(x_1) = F_1(\sin\beta x_1 - \alpha_1 \sinh\beta x_1) \text{ and } \phi_2(x) = F_2(\sin\beta x_2 - \alpha_2 \sinh\beta x_2), \tag{28a,b}$$

where

$$\alpha_1 = \frac{\sin\beta l_1}{\sinh\beta l_1} \text{ and } \alpha_2 = \frac{\sin\beta l_2}{\sinh\beta l_2}. \tag{29a,b}$$

The values of the two coefficients F_1 and F_2 can be found in this case by imposing the continuity of the first and second spatial derivatives of the functions $\phi_1(x_1)$ and $\phi_2(x_2)$ for $x_1=l_1$ and $x_2=l_2$, which are consistent with the use of a force actuator, so that

$$\left.\frac{\mathrm{d}\phi_1(x_1)}{\mathrm{d}x_1}\right|_{x_1=l_1} = -\left.\frac{\mathrm{d}\phi_2(x_2)}{\mathrm{d}x_2}\right|_{x_2=l_2}, \quad \left.\frac{\mathrm{d}^2\phi_1(x_1)}{\mathrm{d}x_1^2}\right|_{x_1=l_1} = \left.\frac{\mathrm{d}^2\phi_2(x_2)}{\mathrm{d}x_2^2}\right|_{x_2=l_2} \tag{30}$$

which gives two homogeneous equations in F_1 and F_2, that could be written in the following matrix form:

$$\begin{bmatrix} \beta(\cos\beta l_1 - \alpha_1 \cosh\beta l_1) & \beta(\cos\beta l_2 - \alpha_2 \cosh\beta l_2) \\ \beta^2(-\sin\beta l_1 - \alpha_1 \sinh\beta l_1) & -\beta^2(-\sin\beta l_2 - \alpha_2 \sinh\beta l_2) \end{bmatrix} \begin{bmatrix} F_1 \\ F_2 \end{bmatrix} = \begin{bmatrix} 0 \\ 0 \end{bmatrix}. \tag{31}$$

Non-trivial solutions for F_1 and F_2 are found by imposing the determinant of the 2×2 matrix to be equal to zero. The values of β that bring to zero the determinant, that will be referred as β_r, give the natural frequencies. Using the definition of β given for Eq. (23), the natural frequencies are then found with the formulae:

$$\omega_r = \beta_r^2 \sqrt{\frac{EI_y}{\rho A}}. \tag{32}$$

The natural modes can then be derived by substituting the values of β_r into Eqs. (28a,b) and (29a,b) so that

$$\phi_1(x_1) = F\sigma_r\big(\sin\,\beta_r x_1 - \alpha_1 \sinh\,\beta_r x_1\big), \tag{33a}$$

$$\phi_2(x_2) = F\big(\sin\beta_r x_2 - \alpha_2 \sinh\beta_r x_2\big), \tag{33b}$$

where

$$\sigma_r = -\frac{\cos\beta_r l_2 - \alpha_2\cosh\beta_r l_2}{\cos\beta_r l_1 - \alpha_1\cosh\beta_r l_1}. \tag{34}$$

The left column of Table 3 gives the first five natural frequencies, calculated using Eq. (32) with the values of β from Eq. (31), of the constrained beam with the collocated velocity sensor and force actuator system together with the five resonance frequencies found in the simulations above. The analytical natural frequencies are quite close to the observed resonance frequencies. Fig. 10 shows the first four natural modes of the constrained beam calculated using formulae (33a) and (33b). The collocated velocity sensor and force actuator control system with large feedback control gains introduces a pinning constraint, as shown in Fig. 6, that changes the modes in such a way as shown in Fig. 10 they are similar to those of two simply supported beams joined at the control position. The calculation of the natural frequencies and natural modes cannot, however, be reduced to that of two simply supported beams.

3.2. Beam with the collocated velocity sensor and moments pair actuator feedback control system

The natural modes of the beam with the closely located velocity sensor and piezoelectric patch actuator can be derived in a similar manner to that used in the previous section. The beam is divided into two bays with the two mirror systems of reference x_1 and x_2 as shown in Fig. 9. For this control case some of the boundary conditions for the two bays are the same as for the previous one, given by Eqs. (25a–c) and (26a–c). Thus the two beam functions $\phi_1(x)$ and $\phi_2(x)$ are given by Eqs. (28a) and (28b), respectively. In this case, however, assuming the length of the

Table 3
Observed resonance and calculated natural frequencies of the beam with either the collocated velocity sensor and force actuator or the closely located velocity sensor and piezoelectric patch actuator control systems with very high feedback control gains

Resonance number	Beam with the velocity sensor and force actuator		Beam with the velocity sensor and piezoelectric patch actuator	
	Resonance frequencies (Hz)	Natural frequencies (Hz)	Resonance frequencies (Hz)	Natural frequencies (Hz)
1	92.8	94.2	54.6	54.4
2	185.7	187.3	117.6	119.2
3	355.6	358.3	276.9	278.8
4	622.5	624.9	498.2	496.4
5	793.3	795.3	681.3	679.4

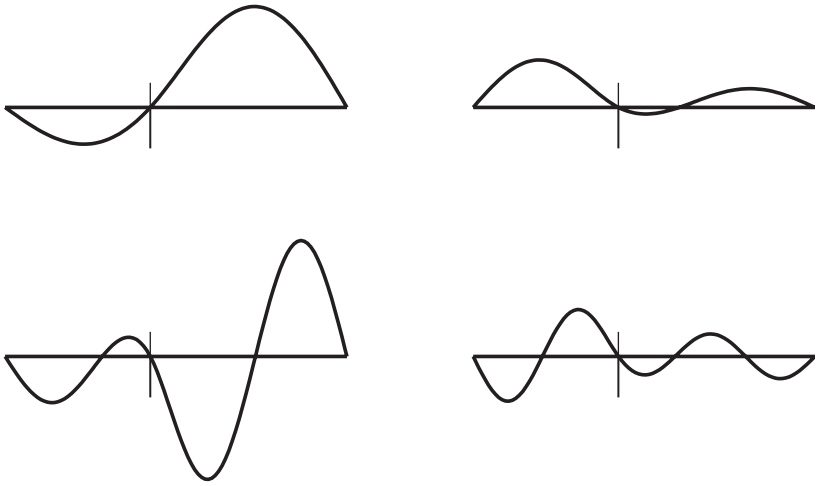

Fig. 10. New natural modes of the constrained beam by the collocated velocity sensor and force actuator feedback control system with a large control gain.

piezoelectric patch actuator to be smaller than the bending wavelength, i.e. $e<\pi/k_B$ where k_B is the bending wavenumber, the bending moments and the shear forces at the two ends of the piezoelectric patch have equal magnitude, but opposite sign in the latter case, so that the two coefficients F_1 and F_2 are then obtained by imposing the following two conditions:

$$\left.\frac{\mathrm{d}^2\phi_1(x_1)}{\mathrm{d}x_1^2}\right|_{x_1=l_1-e} = \left.\frac{\mathrm{d}^2\phi_1(x_2)}{\mathrm{d}x_2^2}\right|_{x_2=l_2-e}, \quad \left.\frac{\mathrm{d}^3\phi_1(x_1)}{\mathrm{d}x_1^3}\right|_{x_1=l_1-e} = -\left.\frac{\mathrm{d}^3\phi_1(x_2)}{\mathrm{d}x_2^3}\right|_{x_2=l_2-e} \tag{35a,b}$$

which gives two homogeneous equations in F_1 and F_2, that could be written in the following matrix form:

$$\begin{bmatrix} -\beta^3(\cos\beta(l_1-e)-\alpha_1\cosh\beta(l_1-e)) & -\beta^3(\cos\beta(l_2-e)-\alpha_2\cosh\beta(l_2-e)) \\ \beta^2(-\sin\beta(l_1-e)-\alpha_1\sinh\beta(l_1-e)) & -\beta^2(-\sin\beta(l_2-e)-\alpha_2\sinh\beta(l_2-e)) \end{bmatrix} \begin{bmatrix} F_1 \\ F_2 \end{bmatrix} = \begin{bmatrix} 0 \\ 0 \end{bmatrix}. \tag{36}$$

Non-trivial solutions for F_1 and F_2 are found by imposing the determinant of the 2×2 matrix to be equal to zero. As discussed in the previous case, the values of β that bring to zero the determinant, that will be referred as β_r, give the natural frequencies so that, using the definition of β given for Eq. (23), the natural frequencies are then found with the formulae

$$\omega_r = \beta_r^2\sqrt{\frac{EI_y}{\rho A}}. \tag{37}$$

Using Eqs. (28a) and (28b) the natural modes of the entire beam are then given by the two following functions:

$$\phi_1(x_1) = F\sigma_r\big(\sin\beta_r x_1 - \alpha_1\sinh\beta_r x_1\big), \tag{38a}$$

$$\phi_2(x_2) = F\big(\sin\beta_r x_2 - \alpha_2\sinh\beta_r x_2\big), \tag{38b}$$

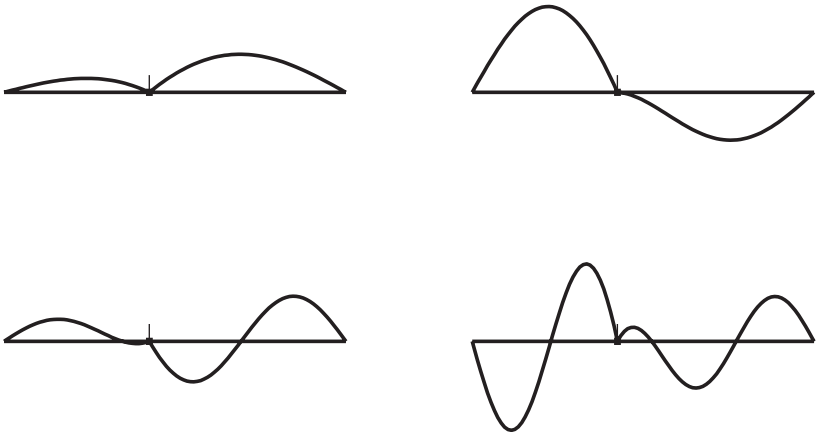

Fig. 11. New natural modes of the constrained beam by the closely located velocity sensor and piezoelectric patch actuator feedback control system with a large control gain.

where

$$\sigma_r = \frac{\cos\beta_r(l_2 - e) + \alpha_2 \cosh\beta_r(l_2 - e)}{\cos\beta_r(l_1 - e) + \alpha_1 \cosh\beta_r(l_1 - e)}. \tag{39}$$

The right column of Table 3 gives the first five resonance frequencies and the first five natural frequencies, calculated using Eq. (37) with the values of β_r from Eq. (36), of the constrained beam with the closely located velocity sensor and piezoelectric patch actuator feedback control system. Also in this case the analytical natural frequencies are quite close to the resonance frequencies as expected for the lightly damped beam systems when the closely located velocity sensor and piezoelectric patch actuator implements large control gains. The first four natural modes of the constrained beam calculated using formulae (38a) and (38b) are shown in Fig. 11. The piezoelectric patch actuator is driven to reduce the vibration of the beam at the error sensor position and, when relatively large control gains are implemented, it holds back the beam at the error sensor position. The reactive actuation mechanism of the piezoelectric patch produces relatively irregular mode shapes as can be seen in Fig. 11. Comparing these four mode shapes with the four plots given in Fig. 8 it is found that also in this case the response of the constrained beam at resonance frequencies is controlled by the new natural modes of the constrained beam.

The results presented in this subsection have also been extended to the case where the length of the piezoelectric patch actuator is not constrained to be smaller than the bending wavelength. An approximate approach is introduced in the appendix that could be used to derive the natural frequencies and natural modes of the simply supported beam when constrained by the control system with large feedback control gains.

4. Concluding remarks

This paper presents a theoretical analysis of the flexural response of a beam with a control system which implements direct velocity feedback, i.e. active damping, using either a

collocated velocity sensor and force actuator or a closely located velocity sensor and piezoelectric patch actuator. The aim of this paper is to analyse the new natural frequencies and natural modes generated by very high control gains of the velocity feedback control system.

The study shows that as the control gain is increased, the vibration of the beam is initially reduced at resonance frequencies because of the active damping effect. However this effect does not continue, at which the vibration of the beam is rearranged into a new set of lightly damped resonance frequencies so that the overall kinetic energy of the beam is increased to the same or even higher values than those of the beam without control systems.

The new natural frequencies and natural modes of the beam constrained by two feedback control systems with either force or moment pair actuation have been derived analytically and good agreement has been found between the values of the new natural frequencies and the resonance frequencies of the controlled beams when large control gains are implemented. Also the new natural mode shapes have been found to be very similar to the vibrations along the beam length at the resonance frequencies of the beams when constrained by large control gains.

Appendix

Following the mode-summation procedures for continuous flexible systems presented by Thomson [25], if the transverse displacement of a beam is expressed in terms of the bending natural modes $\phi_r(x)$ with a series expansion such that

$$w(x,t) = \sum_r \phi_r(x) q_r(t), \tag{A.1}$$

then the generalized coordinates $q_r(t)$ can be determined from the Lagrange's equations

$$\frac{\mathrm{d}}{\mathrm{d}t}\left(\frac{\partial T}{\partial \dot{q}_r}\right) - \frac{\partial T}{\partial q_r} + \frac{\partial D}{\partial \dot{q}_r} + \frac{\partial U}{\partial q_r} = Q_r, \tag{A.2}$$

where the kinetic energy, strain energy and Rayleigh's dissipation functions are, respectively, given in terms of the generalized coordinates as follows:

$$T = \frac{1}{2}\sum_r M_r \dot{q}_r^2, \quad U = \frac{1}{2}\sum_r K_r q_r^2, \quad D = \frac{1}{2}\sum_r C_r \dot{q}_r^2. \tag{A.3a–c}$$

For bending vibration of a beam the generalized mass M_r, stiffness K_r and damping C_r are given by

$$M_r = \int_0^{l_x} \rho A \phi_r^2(x)\,\mathrm{d}x, \quad K_r = \int_0^{l_x} EI_y \left[\phi_r''(x)\right]^2 \mathrm{d}x, \quad C_r = \alpha M_r + \beta K_r. \tag{A.4a–c}$$

with

$$\alpha + \omega_r^2 \beta = 2\zeta_r \omega_r, \tag{A.5}$$

where ω_r and ζ_r are, respectively, the natural frequency and modal damping ratio of the rth natural mode of the beam and $\phi_r''(x) = \partial^2 \phi_r(x)/\partial x^2$. The generalized force Q_r is

given by

$$Q_r = \int_0^{l_x} f_z(x)\phi_r(x)\,\mathrm{d}x + \int_0^{l_x} m_y(x)\phi_r'(x)\,\mathrm{d}x, \tag{A.6}$$

where $f_z(x)$ and $m_y(x)$ are, respectively, the transverse force and bending moment acting along the beam length and $\phi'(x) = \partial\phi(x)/\partial x$. If the beam is excited only by the control force or moments pair as shown in Fig. 1, then the generalized forces will be given, respectively, by

$$Q_r = f_{zc}\phi_r(x_c), \quad Q_r = m_{yc}\psi_r(x_c), \tag{A.7}$$

where $\psi_r(x_c) = \{\phi_r'(x_c - e) - \phi_r'(x_c + e)\}$ and f_{zc} and m_{yc} are, respectively, the control force and control moments generated by the force and piezoelectric patch actuators. If direct velocity feedback is implemented then, according to the block diagram in Fig. 2, $f_{zc} = -h\dot{w}_c$ and $m_{yc} = -h\dot{w}_c$ so that, using the series expansion for $\dot{w}_c$ given by Eq. (A.1),

$$\dot{w}_c(t) = \sum_s \phi_s(x_c)\dot{q}_s(t) \tag{A.8}$$

the generalized forces for the two control cases become

$$Q_r = -h\phi_r(x_c)\sum_s \phi_s(x_c)\dot{q}_s, \quad Q_r = -h\psi_r(x_c)\sum_s \phi_s(x_c)\dot{q}_s. \tag{A.9a,b}$$

Substituting the expressions for the kinetic and strain energies given by Eqs. (A.3a) and (A.3b) and for the generalized forces (A.9a,b) into the Lagrange's Eq. (A.2) the following second-order ordinary differential equations in q_r are derived for the two control cases:

$$\ddot{q}_r + 2\zeta_r\omega_r\dot{q}_r + \omega_r^2 q_r = -\frac{h}{M_r}\phi_r(x_c)\sum_s \phi_s(x_c)\dot{q}_s, \tag{A.10a}$$

$$\ddot{q}_r + 2\zeta_r\omega_r\dot{q}_r + \omega_r^2 q_r = -\frac{h}{M_r}\psi_r(x_c)\sum_s \phi_s(x_c)\dot{q}_s, \tag{A.10b}$$

with $r = 1,\ldots,R$ and $s = 1,\ldots,R$. Considering harmonic motion such that $q(t) = \mathrm{Re}\{q(\omega)\mathrm{e}^{\mathrm{j}\omega t}\}$, then, assuming the time-dependent term $\exp(j\omega t)$ to be implicit in all the following expressions, the two sets of equations can be written in the following matrix form:

$$[\mathbf{A}(\omega)]\{\mathbf{q}(\omega)\} = \{\mathbf{0}\}, \tag{A.11}$$

where the vector $\{\mathbf{q}(\omega)\}$ contains the frequency-dependent generalized coordinates $q_1(\omega)$, $q_2(\omega),\ldots,q_R(\omega)$

$$\{\mathbf{q}(\omega)\} = \begin{Bmatrix} q_1(\omega) \\ q_2(\omega) \\ \vdots \\ q_R(\omega) \end{Bmatrix}, \tag{A.12}$$

and, considering the two control cases, the diagonal and off-diagonal terms of the matrix $[\mathbf{A}(\omega)]$ are given by

$$A_{rr}(\omega) = -\omega^2 + \mathrm{j}\omega\left(2\zeta_r\omega_r + h\frac{\phi_r^2(x_c)}{M_r}\right) + \omega_r^2, \tag{A.13a}$$

$$A_{rr}(\omega) = -\omega^2 + \mathrm{j}\omega\left(2\zeta_r\omega_r + h\frac{\phi_r(x_c)\psi_r(x_c)}{M_r}\right) + \omega_r^2, \tag{A.13b}$$

$$A_{rs}(\omega) = \mathrm{j}\omega h\frac{\phi_r(x_c)\phi_s(x_c)}{M_r}, \tag{A.14a}$$

$$A_{rs}(\omega) = \mathrm{j}\omega h\frac{\phi_r(x_c)\psi_s(x_c)}{M_r}. \tag{A.14b}$$

The damped natural frequencies of the beam with the two DVFB control systems under study are then found by imposing the determinant of the matrix $\mathbf{A}(\omega)$ to be zero:

$$\det\ [\mathbf{A}(\omega)] = 0. \tag{A.14}$$

As described in the paper, for high control gains the beam is constrained to be fixed at the error sensor position x_c and in this case Eq. (A.14) gives the natural frequencies of the constrained beam. The co respective natural modes are then obtained from Eq. (A.1) using the generalized coordinated derived from Eq. (A.11) to within a constant. The natural frequencies and natural modes derived with this formulation for the case of large velocity feedback control gains have been found to be consistent with those found with the analytical formulation presented in Section 3 and with the new resonance frequencies found in the plots given in Figs. 3 and 7 of the total kinetic energy of the beam when very high control gains are implemented.

With this formulation it is possible to better understand two phenomena: first the variation of the natural frequencies and natural modes of the beam with reference to the velocity feedback control gain and second, the active damping effect introduced by the direct velocity feedback control system. If for example the beam with the collocated velocity sensor and force actuator control system is analysed, then considering the terms in the rth row of the matrix $[\mathbf{A}(\omega)]$, one can see that the direct velocity feedback control system introduces on the rth natural mode of the beam R extra damping terms $\mathrm{j}\omega h\sum_{s=1}^{R}\phi_r(x_c)\phi_s(x_c)/M_r$. These extra damping effects can be expressed in terms of modal *active damping ratios*:

$$\delta_{rs} = h\frac{\phi_r(x_c)\phi_s(x_c)}{2M_r\omega_r}, \tag{A.15}$$

which are (a) directly proportional to the control gain, (b) inversely proportional to the natural frequency ω_r and (c) directly proportional to the product of the amplitude of the rth and sth natural modes of the beam at the control position. In this specific case where a collocated sensor and actuator are used, the *self-active damping ratio* δ_{rr} is always positive so that an additional damping effect is generated. In contrast the *mutual active damping ratios* δ_{rs} could be either positive or negative depending on the relative sign of the rth and sth natural modes of the beam at

the control positions [20]. In other words, these mutual active damping ratios will introduce some additional negative or positive damping effects. The extent of these mutual damping effects between two modes is however determined by the amplitudes of the generalized coordinate relative to the two modes themselves. As a result, for each frequency there will be an optimal control gain that will minimize the overall vibration of the beam. If instead the control gain is kept constant with frequency, then, as discussed in Sections 2.1 and 2.2 there will be an overall optimal control gain that produces the best averaged control effect over the frequency band considered.

References

[1] H.F. Olson, Electronic control of noise, vibration, and reverberation, *Journal of the Acoustical Society of America* 28 (1956) 966–972.
[2] J.C. Bleazey, Electronic sound absorber, *Journal Audio Engineering* 10 (1962) 135–139.
[3] T.H. Rockwell, J.M. Lawther, Theoretical and experimental results on active vibration dampers, *Journal of the Acoustical Society of America* 36 (2) (1964) 1507–1515.
[4] A. Preumont, *Vibration Control of Active Structures*, 2nd Ed, Kluwer Academic Publishers, London, 2002.
[5] M.J. Balas, Direct velocity feedback of large space structures, *Journal of Guidance and Control Dynamics* 2 (1979) 252–253.
[6] R.J. Benhabib, R.P. Iwens, R.L. Jackson, Stability of large space structure control systems using positivity concepts, *Journal of Guidance and Control* 4 (5) (1981) 487–494.
[7] S.J. Elliott, P. Gardonio, T.J. Sors, M.J. Brennan, Active vibroacoustic control with multiple local feedback loops, *Journal of the Acoustical Society of America* 111 (2) (2002) 908–915.
[8] E. Bianchi, P. Gardonio, S.J. Elliott, Smart panel with an array of decentralized control systems for active structural acoustic control, ISVR Technical Memorandum No. 886, University of Southampton, UK, 2002.
[9] P. Gardonio, E. Bianchi, S.J. Elliott, Smart panel with an array of decentralized control systems for the control of sound transmission. Part I: theoretical predictions, *Journal of Sound and Vibration* 274 (2004) 163–192.
[10] P. Gardonio, E. Bianchi, S.J. Elliott, Smart panel with an array of decentralized control systems for the control of sound transmission. Part II: design of the decentralized control systems, *Journal of Sound and Vibration* 274 (2004) 193–213.
[11] E. Bianchi, P. Gardonio, S.J. Elliott, Smart panel with an array of decentralized control systems for the control of sound transmission. Part III control system implementation, *Journal of Sound and Vibration* 274 (2004) 215–232.
[12] V. Jayachadran, J.Q. Sun, Unconditional stability domains of structural control systems using dual actuator–sensor pairs, *Journal of Sound and Vibration* 208 (1) (1997) 159–166.
[13] S.E. Burke, J.E. Hubbard Jr., J.E. Meyer, Distributed transducers and collocation, *Mechanical Systems and Signal Processing* 7 (4) (1993) 349–361.
[14] L. Meirovitch, *Dynamics and Control of Structures*, Wiley, New York, 1990.
[15] G. Franklin, J.D. Powell, A. Emami-Naeini, *Feedback Control of Dynamic Systems*, Prentice-Hall, Upper Saddle River, NJ, 2002.
[16] G.D. Martin, On the Control of Flexible Mechanical Systems, Ph.D. Dissertation, Stanford University, CA, 1978.
[17] B. Wie, On the Modelling Control of Flexible Space Structures, Ph.D. Dissertation, Stanford University, CA, 1981.
[18] V.A. Spector, H. Flashner, Sensitivity of structural models for noncollocated control systems, *Journal of Dynamic Systems, Measurement, and Control* 111 (1989) 646–655.

[19] V.A. Spector, H. Flashner, Modelling ad design implications of noncollocated control in flexible systems, *Journal of Dynamic Systems, Measurement, and Control* 112 (1990) 186–193.
[20] D.K. Miu, Physical interpretation of transfer function zeros for simple control systems with mechanical flexibilities, *Journal of Dynamic Systems, Measurement, and Control* 113 (1991) 419–424.
[21] F.J. Fahy, *Sound and Structural Vibration*, Academic Press, London, 1994.
[22] C.R. Fuller, S.J. Elliott, P.A. Nelson, *Active Control of Vibration*, Academic Press, London, 1996.
[23] S. Koshigoe, J.W. Murdock, A unified analysis of both active and passive damping for a plate with piezoelectric transducers, *Journal of the Acoustical Society of America* 93 (1) (1993) 346–355.
[24] S. Timoshenko, D.H. Young, W. Weaver Jr., *Vibration Problems in Engineering*, 4th ed., Wiley, London, 1992.
[25] W.T. Thomson, *Theory of Vibration with Applications*, Prentice-Hall, London, 1993 (reprinted by Stanley Thornes Ltd., 1998).